

Visible-light photon migration through myocardium in vivo

AMIR H. GANDJBAKHACHE,¹ ROBERT F. BONNER,¹
ANDREW E. ARAI,² AND ROBERT S. BALABAN²

¹Laboratory of Integrative and Medical Biophysics, National Institute of Child Health and Human Development, and ²Laboratory of Cardiac Energetics, National Heart, Lung, and Blood Institute, National Institutes of Health, Bethesda, Maryland 20892

Gandjbakhche, Amir H., Robert F. Bonner, Andrew E. Arai, and Robert S. Balaban. Visible-light photon migration through myocardium in vivo. *Am. J. Physiol.* 277 (*Heart Circ. Physiol.* 46): H698–H704, 1999.—Empirical data between 510 and 590 nm of diffuse reflected light from the pig heart in vivo have shown that myoglobin and cytochrome *c* absorption peaks with little apparent contribution of red blood cell (RBC) Hb. Monte Carlo simulations of photon migration in tissue were performed to compare the effects of myoglobin and cytochromes with those of blood Hb on photon pathlengths and diffuse reflectance of visible wavelengths (450–600 nm) from the pig heart in vivo. Wavelength dependence of the input parameters, including the transport-corrected scattering coefficients ($1.1\text{--}1.2\text{ mm}^{-1}$) and the absorption coefficients of blood-free solubilized heart tissue ($0.43\text{--}1.47\text{ mm}^{-1}$), as well as the absorption coefficients of Hb, were determined by an integrating sphere method and standard spectrophotometry, respectively. The Monte Carlo simulations indicate that in the 510- to 590-nm range the mean path length within the myocardium for diffusely reflected light varies from 1.4 to 1.2 mm, whereas their mean penetration depth within the epicardium is only 330–400 μm for blood-free heart tissue. Analysis shows that the blood Hb absorption extrema are only observable between 510 and 590 nm when RBC concentration in tissue is $>0.5\%$. Blood within vessels much larger than capillaries does not contribute significantly to the spectral features, because virtually all light in this spectral range is absorbed during transit through large vessels ($>100\text{ }\mu\text{m}$). This analysis suggests that diffuse reflected light in the 510- to 590-nm region will show spectral features uniquely associated with myoglobin and cytochrome *c* oxygenation states within 400 μm of the surface of the heart in situ as long as the capillary RBC concentration remains $<0.5\%$.

myoglobin; hemoglobin; cytochromes; hematocrit; pig; oxygen; Monte Carlo simulations; photon migration

WITH THE USE OF THE VISIBLE-LIGHT spectrum, information on numerous aspects of the tissue milieu and biochemistry can be ascertained. This information includes myoglobin and Hb oxygenation as well as the mitochondrial cytochrome redox state (9, 15). However, most biological tissues are optically highly turbid in the visible wavelengths. Thus interpretation of the reflection spectrum of tissue is critically dependent on scattering as well as absorption. The path length and penetration depth distributions in the tissue of the detected photons vary markedly with scattering and absorption changes. Researchers have attempted to use

theoretical models to separate the effects of absorption and scattering in reflection spectroscopy. These models, once implemented as an “inverse problem” are supposed to quantify the absorbance spectra of different biological species (e.g., Hb, cytochromes). The first model, proposed by Caspary et al. (5) and Hoffmann and Lubbers (12), is the Kubelka-Munk theory (2 flux and higher) describing a one-dimensional diffusion process through different layers of tissue. Recently, three-dimensional models describing photon migration within tissue, such as the random walk theory (3, 7) or the diffusion approximation to the transport equation (13), have been proposed. However, all these diffusion-like models fail to represent the behavior of photons with very short path lengths ($<2\text{ mm}$). Indeed, when tissue absorption and scattering coefficients are similar, as in the 510- to 590-nm wavelength range, the detected photons are those that experienced only few scattering events and only penetrate to superficial depths.

An alternative model in such cases is the stochastic numerical Monte Carlo (MC) method, in which photon trajectories are simulated in tissue (8, 11). Although MC simulations are the most accurate tools to describe diffusion-like processes in tissue, they cannot be used efficiently to retrieve the spectral features from spectroscopic measurements. Their primary use has been to test analytic models and in forward solutions, i.e., when the optical characteristics of the medium are known a priori. The purpose of the present study is to evaluate the path length and spectral characteristics of visible light in reflection spectroscopic studies of the heart in vivo described previously (2).

MC simulations follow the migration of a statistically representative number of individual photons after they enter the medium and record the paths of only those photons that reemerge from the tissue and are detected. In NUMERICAL ANALYSIS, we describe the numerical analysis on which our simulations are performed. The characterization of photon movements within a tissue requires specification of the measurement geometry and the three pertinent tissue optical properties: the scattering coefficient (inverse of the mean free path), the coefficient of scattering anisotropy, and the absorption coefficients of the tissue and the blood. In RESULTS, we present pathlength analysis obtained from our simulations of actual in situ experiments (2) with use of in vitro absorbance measurements of homogenized heart tissue and Hb at the wavelengths of interest. Also, the scattering coefficient of blood-free pig heart tissue is measured using an integrating sphere method. A mathematical model of light interaction with the capillary bed is also described. Finally, with the use

The costs of publication of this article were defrayed in part by the payment of page charges. The article must therefore be hereby marked “advertisement” in accordance with 18 U.S.C. Section 1734 solely to indicate this fact.

of these input parameters, reflectance spectra of heart tissue at 450–600 nm for three different myocardial blood volumes are obtained and compared with reflectance spectra of in vivo pig heart.

NUMERICAL ANALYSIS

An MC simulation program has been written in Fortran to interpret the experimental results obtained from our in vivo reflectance spectroscopic measurements of pig heart. The program has the following features. Photons are inserted with a given angle (α) at the surface of a semi-infinite (here ≥ 1 cm) scattering medium. The incident direction within the tissue is corrected for refraction at the air-surface interface [index of refraction of myocardium (n_{tissue}) = 1.4]. The path length between collisions is determined by comparing a randomly generated number between 0 and 1 with the cumulative probability distribution for an exponentially distributed scattering length (P_{cum}) = $1 - \exp(-l)$ and taking the scattering length to be that value of l_t for which P_{cum} equals the selected random number (i.e., Beer’s law of scattering). The azimuthal angle (φ) is randomly selected between 0 and 2π . Because scattering in tissues is intrinsically strongly peaked in the forward direction, the polar angle (θ) is similarly determined from the cumulative probability distribution of the Henyey-Greenstein phase function, which is widely used to represent the anisotropy in tissues (10)

$$F(\theta) = \frac{1 - g^2}{2g} \left[\frac{1}{1 - g} - \frac{1}{(1 + g^2 - 2g \cos \theta)^{1/2}} \right] \quad (1)$$

where g is the anisotropy coefficient, defined as the mean value of $\cos \theta$ ($g = \langle \cos \theta \rangle$), and $0 \leq \theta \leq \pi$. The polar and azimuthal angles are sampled in the reference frame of the incident and resultant directions of photon propagation.

The simulations follow the migration of individual photons after they enter the tissue and keep track of their path lengths and their maximum penetration depths as they emerge on the surface. The direction of emergence of each photon from the surface is computed and corrected for tissue-air refractive index mismatch. Only those photons that emerge within a given cone with an angle δ (defined by the experimental setup) are recorded in a two-dimensional matrix ($\Lambda_{d,l}$), the elements of which are the number of photons reemitted having d penetration depth, and executed a trajectory with a total optical path length of l . The matrix Λ has 100×100 elements, and the bin sizes (mesh) of the matrix were scaled according to the value of l_t . In the first step the simulations are performed by neglecting internal absorption, which was introduced later to facilitate rapid analysis of wavelength-dependent absorption. To limit computational time, we have specified a maximum path length after which a photon is considered lost if it has not reached the surface. Those photons that have trajectories less than the maximum path length but penetrate deeper than the maximum

depth and/or have a path length greater than the maximum path length assigned to the bins of Λ are recorded in the last bins of the matrix (in all cases the assignment of appropriate absorption attenuates these “overflow” matrix elements to negligible values).

From the elements of the matrix [$\Lambda_{d,l}$], one can derive the path length distribution

$$P(l) = \sum_d \Lambda_{d,l} \quad (2)$$

and the penetration depth distribution

$$D(d) = \sum_l \Lambda_{d,l} \quad (3)$$

The mean path length and the mean penetration depth are obtained by taking the first moments of $P(l)$ and $D(d)$

$$\langle l \rangle = \frac{\sum_l P(l) \cdot l}{\sum_l P(l)} \quad \text{and} \quad \langle d \rangle = \frac{\sum_d D(d) \cdot d}{\sum_d D(d)} \quad (4)$$

One important quantity of interest is $R(\lambda)$, the total reflectance from the tissue at a given wavelength (λ). This quantity is the sum of all photons reflected from the surface subjected to the constraints described previously [e.g., photons reflected in the angular cone (δ)] divided by the total number of injected photons in the simulations (N) and is obtained simply as follows

$$R(\lambda) = \frac{\sum_l P(l)}{N} \quad (5)$$

Effects of Tissue Absorption

From the spectroscopic measurements of homogenized heart tissue described previously (2), one can obtain the absorption coefficient (μ_m , in mm^{-1}), defined as $1/e$ attenuation of the light traveling through the myocardium. The effect of such absorption can be introduced in our simulations by multiplying the elements of $\Lambda_{d,l}$ by $\exp(-\mu_m l)$, which leads to a new two-dimensional matrix containing the effects of tissue absorption. All other quantities may be obtained as described above. In Fig. 1, μ_m values for pig heart tissue, without consideration of Hb absorption, are shown as a function of wavelength (450–600 nm). Values chosen at 5-nm intervals are used in our calculations.

Effects of Red Blood Cell Absorption

Another component that absorbs light is the Hb within red blood cells (RBCs) in the vasculature. A set of spectroscopic measurements was performed on lysed RBCs described previously (2). Optical densities of Hb at different wavelengths are then obtained. With the assumption that the mean optical path through an

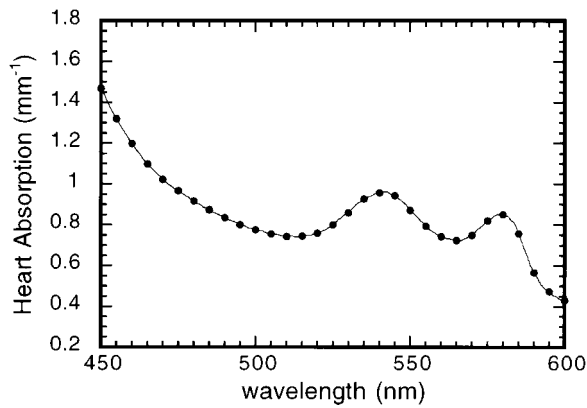


Fig. 1. Absorption coefficients (solid line, μ_m) of pig heart tissue, without consideration of Hb absorption, as a function of wavelength (450–600 nm). ●, Values chosen at 5-nm intervals.

RBC is 6 μm (i.e., its mean diameter), the transmittance (T_{rbc}) for a single cell can be calculated. This spectrum is presented as a function of wavelength (450–600 nm) at 5-nm intervals in Fig. 2. In Fig. 2, in the wavelength range of interest, the transmission of light through a single RBC varies between 80 and 90%. Absorption of light by RBCs has different effects on the tissue reflectance spectra depending on the size of the vessel containing them (e.g., whether the probability of absorption within an RBC is associated with absorption in many neighboring cells within the same vessel).

First, let us analyze the contribution of blood in the capillary bed to the overall reflectance spectra. When light is transmitted through a particulate suspension such as RBCs in plasma, “sieving effects” (14) require accounting for the probability of missing the particulate absorbers. With multiple scattering within tissues, which randomizes the direction of photons, we describe the number of interactions of light with the RBCs by a probability distribution derived previously to quantify Doppler shifts by moving RBCs within turbid tissues (4). In laser-Doppler flowmetry, the light penetration depth is limited by small source-detector separations to depths similar to those in the present case of high tissue absorption. In this model the probability of m

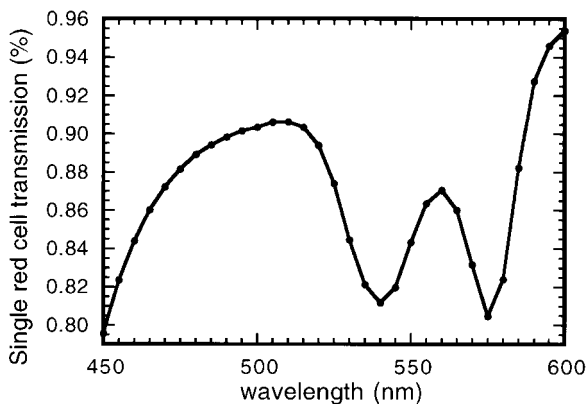


Fig. 2. Single red blood cell (RBC) transmission spectra as a function of wavelength (450–600 nm) at 5-nm intervals.

(varying from zero to infinity) interactions with RBCs is represented by a Poisson distribution

$$P(m) = \frac{(\bar{m})^m \exp(-\bar{m})}{m!} \quad (6)$$

where \bar{m} is the average number of interactions for a given path length and is equal to (see Eq. 4)

$$\bar{m} = \sum_{\text{rbc}} \cdot c \cdot l \quad (7)$$

where Σ_{rbc} is the cross section of a single cell, c is the volume concentration of cells, and l is the path length. As expected, the mean number of interactions is directly proportional to the concentration of RBCs in the capillary bed and the path length.

The corresponding distribution of light attenuation due to RBCs then becomes

$$A(m) = \frac{(T_{\text{rbc}}\bar{m})^m \exp(-\bar{m})}{m!} \quad (8)$$

Averaging over all possible values of m , one obtains the average attenuation

$$\bar{A}(\bar{m}, T_{\text{rbc}}) = \exp[-(1 - T_{\text{rbc}})\bar{m}] \quad (9)$$

One can replace \bar{m} using Eq. 7. The resulting attenuation for a given path length becomes

$$\bar{A} = \exp(-A_{\text{rbc}} \cdot \Sigma_{\text{rbc}} \cdot c \cdot l) \quad (10)$$

where $A_{\text{rbc}} = (1 - T_{\text{rbc}})$ is the fraction of light absorbed by a single cell. The product $A_{\text{rbc}} \cdot \Sigma_{\text{rbc}} \cdot c$ expressed in mm^{-1} can be seen as the blood (in the capillary bed) absorption coefficient (μ_{H}). In Fig. 3, values of μ_{H} for $c = 0.5$ and 1% and $c = 2\%$ RBC [these values of c bracket the assumed normal value of 1% RBC; the 1% RBC value is derived from a capillary hematocrit of 12% (1) and 8% capillary vol/tissue vol in pig heart] and for an RBC diameter of 6 μm are shown as a function of wavelength (450–600 nm) at 5-nm intervals.

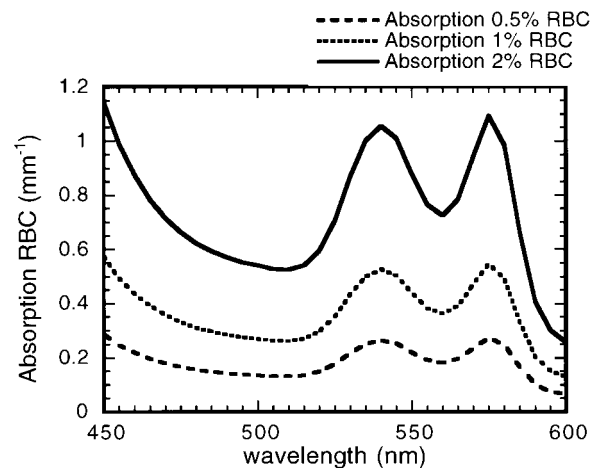


Fig. 3. Absorption coefficients of hemoglobin (μ_{H}) for 3 RBC concentrations (0.5, 1, and 2%) as a function of wavelength (450–600 nm).

We estimated the spectral contribution of the light absorption by large vessels and compared it with the amount of light that interacts with the heart tissue and the capillary bed. The larger vessels ($>25\ \mu\text{m}$) comprise a smaller volume fraction of the myocardium than the capillaries (17). Furthermore, the larger path in transiting such vessels leads to multiple interactions with RBCs. For instance, light entering a large vessel ($\sim 120\ \mu\text{m}$ diameter) will have, on average, 20 interactions with RBCs before it escapes and, therefore, will be highly attenuated (especially at wavelengths between 450 and 590 nm), thus reducing its contribution to the reflectance spectra from the myocardial surface. Using the transmittance spectra for a single cell in Fig. 2, one can estimate the transmission spectrum of light transiting such large vessels as a function of diameter. In Fig. 4, we compare the transmission per 100- μm path in myocardium, neglecting the vascular blood with the transmission per 100- μm path in myocardial tissue containing $>25\text{-}\mu\text{m}$ blood-filled vessels with the density reported by White et al. (17). The low density of larger vessels decreases the overall transmission (or reflectance) slightly but does not cause a measurable shift in absorption maxima associated with myoglobin and cytochrome *c* in the myocardium in the wavelength range of 510–590 nm. Particularly for very short path lengths ($\leq 2\ \text{mm}$; see RESULTS), the fraction of light interacting with large vessels will have a negligible effect on the reflectance spectra. Therefore, we assume that the dominant contribution of Hb in the overall spectra comes from those photons interacting with RBCs within the capillary bed.

With the use of Eq. 10, effects of Hb absorption are introduced into the two-dimensional matrix, as described above, and from the resulting path length distributions, one can derive $R(\lambda)$ of detected photons.

Input parameters in MC simulations. On the basis of the geometry of the experimental setup described previously (2), the average angle of incidence of the light to

the tissue (α) was chosen to be 45° , and the aperture of the collection angle (δ) was set to 30° . The critical parameter in these simulations is the mean free path of photons and the anisotropy coefficient g . The scattering coefficient of tissues, defined as the inverse of the mean free path, varies very slightly as a function of wavelengths of interest (450–600 nm). However, it is important to assign a reasonable average value for l_t for myocardium.

In our previous work (1, 6), we used random walk methodology for determining optical properties of tissue from reflection and transmission measurements performed by an integrating sphere. Briefly, for transmission measurement, a tissue sample and its glass holder are placed in front of the entrance port of an integrating sphere. The laser light illuminates the tissue surface, and the fraction of light transmitted through the sample is collected by the detector of the integrating sphere located perpendicular to the entrance and exit port of the sphere. The reflection from the sample is obtained by placing the tissue sample at the exit port of the sphere and narrowing the entrance port to just accommodate the laser beam. After calibration for losses from the ports and the detector area, the total reflection and transmission from the tissue sample are calculated. These values are then introduced into our iterative inverse algorithm to calculate the absorption and the corrected scattering coefficients of the tissue. Details of this methodology concerning the calibration of the apparatus and the mathematical construct of the inverse method are described elsewhere (1, 6).

The corrected scattering coefficient is the inverse of the mean free path times $(1 - g)$. Thus, using a common estimate of $g = 0.9$ for tissues in these wavelengths, one can obtain the mean free path from the calculated value of the corrected scattering coefficient.

Fresh specimens of pig heart tissue were used to measure the mean free path of the heart at 544 and 594 nm. All animal protocols were approved by the Animal Care and Use Committee of the National Institutes of Health and conform to the standards of the American Physiological Society. Domestic swine were premedicated with ketamine, xylazine, and butorphanol (Torbugesic) administered intramuscularly. Anesthesia was induced with α -chloralose (10 g/l, 10–15 ml/kg iv). After midline thoracotomy, the animal was heparinized (10,000 U iv). The heart was arrested with 20 meq KCl intravenously and rapidly excised. The coronary arteries were immediately perfused with ice-cold saline (~ 1 liter) until no blood was evident in the effluent and blood appeared flushed from the coronary veins. Right and left ventricular free walls were dissected to allow flattening between glass plates for the measurements. The harvested tissues were placed on the holder with uniform thickness of 5.8 mm. Several measurements were performed on different locations of the tissue slab to estimate the heterogeneity of the specimen. The calculated total reflectances and transmittances were then introduced in our inverse algorithm to calculate the optical properties. The corrected scattering coeffi-

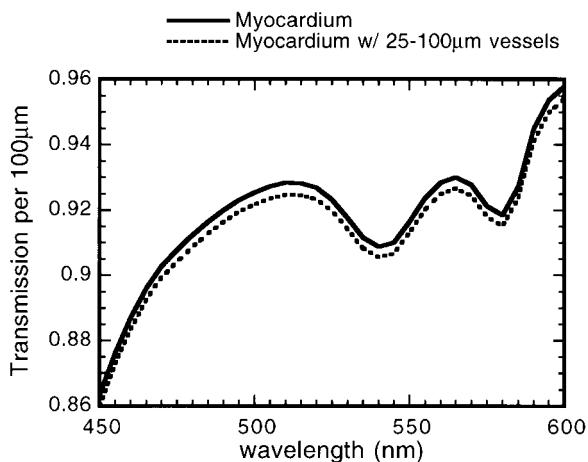


Fig. 4. Transmission spectra through 100 μm of heart tissue (solid line) and through 100 μm of heart tissue with 25–100 μm of vessels (dotted line), with vessel density calculated by Patterson et al. (13). Blood content in these vessels has insignificant effect on extremes of myocardial spectra.

cient was $1.19 \pm 0.08 \text{ mm}^{-1}$ at 544 nm and $1.11 \pm 0.1 \text{ mm}^{-1}$ at 594 nm. For $g = 0.9$, the mean free paths of photons in these two wavelengths are 84 and 90 μm , respectively. In our simulations, we have chosen the largest measured value of 100 μm for the mean free path, allowing the photons to have the longest possible trajectory and greater interactions with RBCs.

RESULTS

With these input parameters, a set of MC simulations was performed, with background absorption equal to zero, by launching 10^6 photons. The maximum path length was set to 2 cm. As described in NUMERICAL ANALYSIS, from the two-dimensional matrix obtained from our simulations, one can introduce the effects of myocardial absorption and of Hb within the vasculature. In Fig. 5A the path length distributions of light diffusely reflected from the epicardial surface at 550

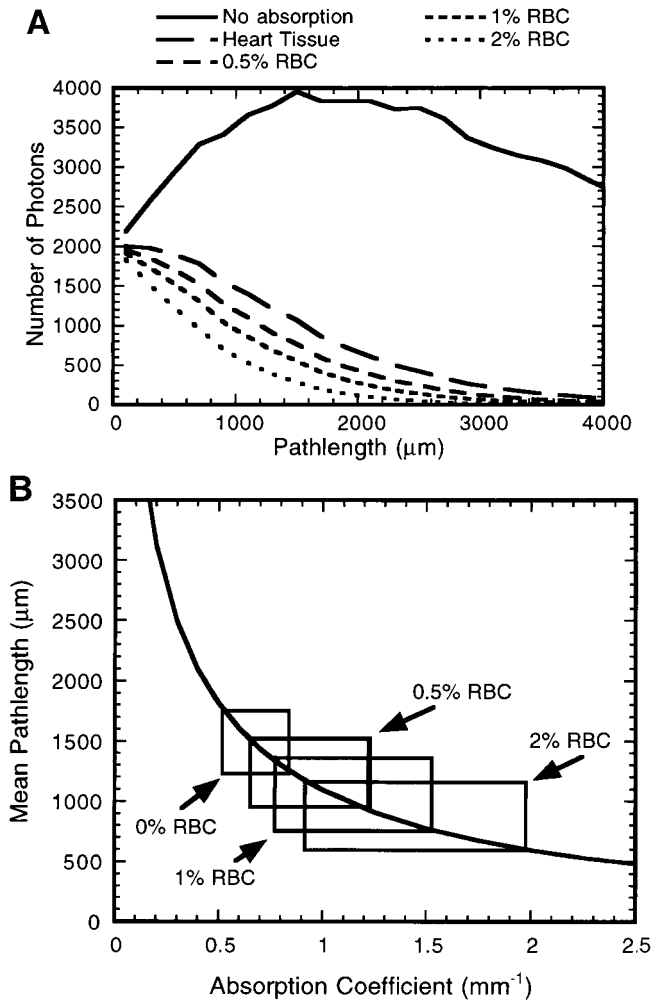


Fig. 5. A: path length distributions of light diffusely reflected from epicardial surface at 550 nm, including no capillary blood volume, and for 3 RBC concentrations (dotted lines). Solid line, path length distribution when no absorption is taken into account. B: mean path length as a function of absorption coefficient of tissue. Mean path length decreases with increasing absorption, which is dependent on capillary RBC volume fraction and wavelength. Range of absorption coefficients for 510- to 590-nm wavelengths for 4 cases (tissue without blood and tissue with 0.5, 1, and 2% RBC) is indicated.

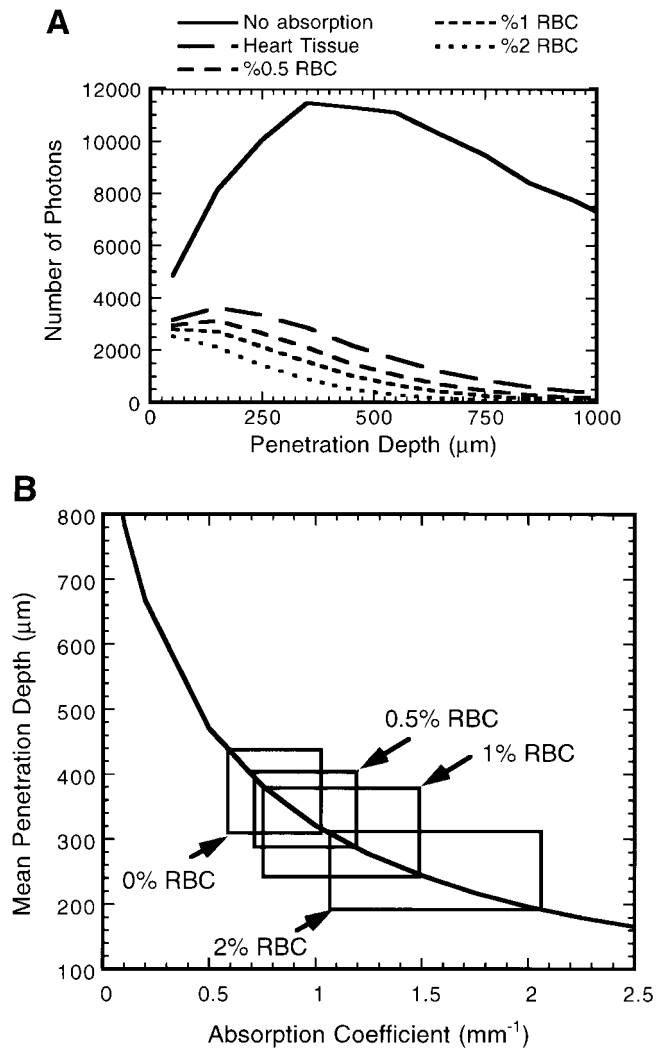


Fig. 6. A: penetration depth distributions at 550 nm. Dotted lines, distributions for 4 cases (tissue without blood and tissue with 0.5, 1, and 2% RBC), which show that deeper photons are preferentially absorbed with increasing capillary blood volume, similar to effects on longer path lengths shown in Fig. 5A. Solid line, penetration depth distribution with no absorption. B: mean penetration depths as a function of tissue absorption coefficient. Range of absorption coefficients for 510- to 590-nm wavelengths for 4 cases (tissue without blood and tissue with 0.5, 1, and 2% RBC) is indicated.

nm are shown, including no capillary blood volume, and for three RBC concentrations described in Fig. 3. The mean path length decreases, as shown in Fig. 5B, with increasing absorption, which is dependent on capillary RBC volume fraction and wavelength. In Fig. 5B, the range of absorption coefficients for 510- to 590-nm wavelengths for four cases (tissue without blood and tissue with 0.5, 1, and 2% RBC) is indicated. For these four cases, the mean path lengths range from 1,150 to 1,675, 900 to 1,500, 780 to 1,350, and 670 to 1,150 μm , respectively. In Fig. 6A the penetration depth distributions at 550 nm show that the deeper photons are preferentially absorbed with increasing capillary blood volume, similar to effects on longer path lengths shown in Fig. 5A. In Fig. 6B the range of mean penetration depths between 510 and 590 nm decreases with increas-

ing capillary RBC concentration. Given the range of absorption coefficients between 510 and 590 nm for these four cases, the mean penetration depths range from 450 to 320, 410 to 280, 380 to 250, and 320 to 200 μm , respectively. For these wavelengths, MC simulations show that the ratio of the mean depth to the mean penetration depth varies between 0.53 and 0.51. Thus one can assert that the light is nearly uniformly distributed within the indicated tissue layers (i.e., the mean penetration depths correspond to layers uniformly sampled by our reflectance measurements).

Now, using values of μ_m presented in Fig. 1 and those of μ_H for $c = 0.5, 1,$ and 2% presented in Fig. 3, one can calculate the wavelength-dependent path length distributions for the case of heart tissue without any blood and those distributions when effects of Hb are added for the three concentrations. From those distributions, one can calculate $R(\lambda)$. These results are shown in Fig. 7, in which we have analyzed the behavior of $R(\lambda)$ with respect to the extremes (minima and maxima) of the heart absorption and those of Hb. Four extremes of myoglobin and cytochromes at 510 and 540 nm (associated with myoglobin and cytochrome *c*), 565 nm (associated with myoglobin and cytochrome *b/c*), and 580 nm (associated with myoglobin) were considered (solid lines). For 0.5% RBC, all these extremes can be seen in the reflection data. However, for 1 and 2% RBC, only the minimum at 540 nm (which is also a minimum in the Hb absorption) is seen. On the other hand, for the extremes of Hb at 540, 560, and 575 nm (dotted lines), for 0.5% RBC, except at 540 nm (which is a minimum of blood free heart tissue), the reflection coefficient does not show any extreme associated with Hb. Whereas for 2% RBC, all the extremes of Hb can be detected clearly in the reflectance spectra. For 1% RBC, the extremes are less clearly associated with blood or blood-free heart tissue. Thus one can assert that, in the range of wavelengths 510–590 nm, spectroscopy of heart tissue with $\leq 0.5\%$ volume fraction of capillary RBCs does not show the spectroscopic signatures of Hb but, rather, those of myocardial Hb and cytochrome *c*.

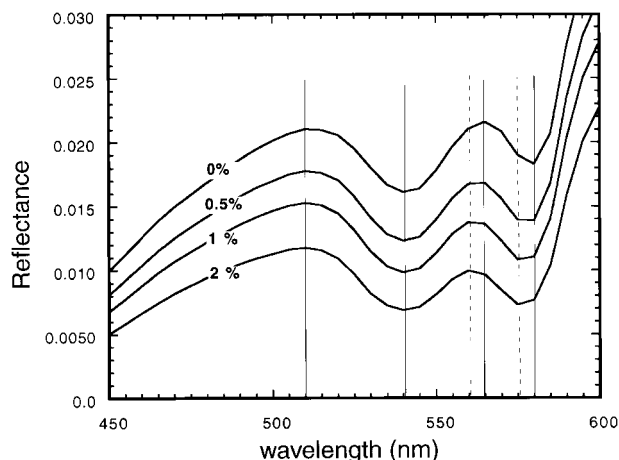


Fig. 7. Diffuse reflectance spectra computed from simulation experiments for 4 cases (tissue without blood and tissue with 0.5, 1, and 2% RBC). Spectral signatures of Hb are not seen for 0.5% RBC.

DISCUSSION

We previously (2) showed that, between 510 and 590 nm, reflection spectroscopy data obtained from the surface of the heart provided insight into the cytosolic myoglobin oxygenation and cytochrome *c* redox state without significant interference from blood Hb. The purposes of the present study were to determine the thickness of the epicardial layer interrogated by these in vivo studies and evaluate the influence of blood volume on the spectral characteristics of diffusely reflected light that has migrated within the epicardial tissue.

Reflection spectroscopy is performed by impinging light on tissue and then analyzing the emitted light. The incoming photons have several fates. Photons can be specularly reflected off the surface of the heart with no spectral information. Generally, these photons are avoided by geometrically constraining the light paths to avoid specular reflection (2). Those photons entering the tissue are multiply scattered and may undergo absorption by the tissue chromophores or blood cells, with “surviving” photons escaping for subsequent detection. Few photons entering larger vessels ($>100 \mu\text{m}$) escape absorption, and therefore insignificant numbers contribute to reflected light spectral features within this wavelength range. For somewhat smaller vessels with luminal diameters between 25 and $100 \mu\text{m}$ within the epicardium, we have shown that for reported number densities the spectral contribution is also insignificant. Because of high scattering and absorption of the myocardial tissue between 510 and 590 nm, the mean path length of the detected photons is very short, on the order of 1 mm. This short path length results in a low probability of encountering the highly dispersed RBCs in the capillary network, which make up $<1\%$ of the tissue volume (see below). This effect minimizes the influence of blood Hb spectral characteristics in the observed reflectance spectrum. The mean penetration depth was estimated to be ~ 0.35 mm. This suggests that, with a 1-cm-diameter surface aperture, the volume interrogated corresponds to $\sim 0.035 \text{ cm}^3$ of the epicardium evaluated by 510- to 590-nm light with the geometry used in our study.

This analysis suggests that the capillary blood content is critical in the determination of path length and spectral characteristics of the collected light. We estimated the RBC influence within the epicardium by comparing the spectral characteristics of the in vivo data with the simulated data while varying RBC content. It was assumed that most of the RBC interactions with the detected light occurred in the capillary bed. Previous studies have determined the hematocrit in the capillaries to be on the order of 12% (15) on the basis of morphological measures in quick-frozen samples from the rat. This yields a 1% volume ratio of RBC to tissue if the capillary volume is 8% in the pig (17). However, the in vivo spectral characteristics are consistent with a capillary RBC volume ratio of $\leq 0.5\%$ on the basis of the MC simulations and Hb titration of heart homogenates (2). These data suggest a capillary hema-

tocrit (<6%) in the pig heart in vivo that is lower than that estimated from the quick-frozen sections of the rat heart. The pig heart data may be lower because of species differences, the low hematocrit of young pigs (~30%) compared with that of the adult rat (~45%), and differences between nondestructive measures and histology section analysis.

In summary, these simulations suggest that the capillary RBC volume is $\leq 0.5\%$ of the superficial myocardium. With use of this blood volume, the mean path length of light at 550 nm is 1–1.5 mm. The mean penetration depth of light is 0.4–0.3 mm.

Address for reprint requests and other correspondence: R. S. Balaban, Laboratory of Cardiac Energetics, National Heart, Lung, and Blood Institute, National Institutes of Health, Bldg. 10, Rm. B1D416, MS 1016, Bethesda, MD 20892 (E-mail: rsb@zeus.nih.gov).

Received 26 February 1998; accepted in final form 22 February 1999.

REFERENCES

1. **Agah, R., A. H. Gandjbakhche, M. Motamedi, R. Nossal, and R. F. Bonner.** Dynamics of temperature-dependent optical properties of tissue. *IEEE Trans. Biomed. Eng.* 43: 839–846, 1996.
2. **Arai, E. A., C. E. Kassera, and P. R. Territo, A. H. Gandjbakhche, and R. S. Balaban.** Myocardial oxygenation: optical spectroscopy of myoglobin and mitochondrial cytochrome in porcine heart in vivo. *Am. J. Physiol.* 277 (*Heart Circ. Physiol.* 46): H683–H697, 1999.
3. **Bonner, R. F., R. Nossal, S. Havlin, and G. H. Weiss.** Model for photon migration in turbid biological tissue. *J. Opt. Soc. Am. A* 4: 423–432, 1987.
4. **Bonner, R. F., and R. Nossal.** Principles of laser-Doppler flowmetry. In: *Laser Doppler Flowmetry*, edited by A. P. Shepherd, Jr., and P. A. Oberg. Boston, MA: Kluwer Academic, 1990, p. 17–45.
5. **Caspary, L., J. Hoffmann, H. R. Ahmad, and D. W. Lubbers.** Multicomponent analysis of reflection spectra from the guinea pig heart for measuring tissue oxygenation by quantitative determination of oxygen saturation of myoglobin and of the redox state of cytochrome *aa₃*, *c*, and *b*. *Adv. Med. Biol.* 191: 263–270, 1985.
6. **Gandjbakhche, A. H., R. Nossal, R. Agah, M. Motamedi, and R. F. Bonner.** Random walk methodology for determining optical properties of tissue from reflection and transmission measurements. *Soc. Photo-Opt. Instrumentation Eng. Proc.* 2391: 273–282, 1995.
7. **Gandjbakhche, A. H., and G. H. Weiss.** Random walk and diffusion-like model of photon migration in turbid media. In: *Progress in Optics*, edited by E. Wolf. Amsterdam: Elsevier Science, 1995, vol. 34, p. 333–402.
8. **Gandjbakhche, A. H., R. Nossal, and R. F. Bonner.** Scaling relationships for theories of anisotropic random walks applied to tissue optics. *Appl. Opt.* 32: 506–516, 1993.
9. **Hassinen, I. E., J. K. Hiltunen, and T. E. S. Takata.** Reflectance spectrophotometric monitoring of the isolated perfused heart as a method of measuring the oxidation-reduction state of cytochromes and oxygenation of myoglobin. *Cardiovasc. Res.* 15: 86–91, 1981.
10. **Henye, L. G., and J. L. Greenstein.** Diffuse radiation in the galaxy. *Astrophysics* 93: 70–83, 1941.
11. **Hoffmann, J., F. Hannebauer, and D. W. Lubbers.** Simulation of the optical properties of an absorbing and scattering medium using the Monte-Carlo technique compared with two- and six-flux theories. *Adv. Med. Biol.* 191: 883–888, 1985.
12. **Hoffmann, J., and D. W. Lubbers.** Quantitative analysis of reflection spectra: evaluation of simulated reflection spectra. *Adv. Med. Biol.* 191: 889–897, 1985.
13. **Patterson, M. S., B. C. Wilson, and B. Chance.** Time-resolved reflectance and transmittance for the noninvasive measurements of tissue optical properties. *Appl. Opt.* 28: 2331–2336, 1989.
14. **Pries, A. R., G. Kansow, and P. Gaetgens.** Microphotometric determination of hematocrit in small vessels. *Am. J. Physiol.* 245 (*Heart Circ. Physiol.* 14): H167–H177, 1983.
15. **Silverman, D. A., and K. Rakusan.** Red blood cell spacing in rat coronary capillaries during the cardiac cycle. *Microvasc. Res.* 52: 143–156, 1996.
16. **Tamura, M., N. Oshing, B. Chance, and I. A. Silver.** Optical measurements of intracellular oxygen concentrations of rat heart in vitro. *Arch. Biochem. Biophys.* 191: 18–22, 1978.
17. **White, F. C., Y. Nakataki, L. Nimmo, and C. M. Bloor.** Compensatory angiogenesis during progressive right ventricular hypertrophy. *Am. J. Cardiovasc. Pathol.* 4: 51–68, 1992.